Slow electron capture by H^+ from initially excited p states of alkali-metal atoms: Effects of alignment and orientation

Bidhan C. Saha
Department of Physics, Florida A&M University, Tallahassee, Florida 32307

Anil Kumar
Department of Physics, J.P. University, Chapra 841 301, India

(Received 6 March 2000; published 15 June 2001)

The state-selective charge transfer for H^+ colliding with the resonantly excited alkali-metal targets (Na and K), along with their dependence on the initial alignment of the electron-charge cloud, has been reported in the low-energy region employing a semiclassical, impact-parameter, close-coupling approach based on the molecular-state expansion augmented with the plane-wave electron translation factor. Although these colliding pairs possess a pseudo-one-electron behavior, they exhibit quite different characteristics. A systematic change in various parameters is observed as we move along the target in the isoelectronic series. The anisotropy parameters $A(2)$ and $A(3)$ for both Na and K atoms are presented. We also report the anisotropy parameters for populating the excited states of Na and K target. For Ly-α emission, in the case of H^+-Na$(3p)$ collisions, our low-energy results agree closely with the quantal calculations [H. Croft and A. S. Dickinson, J. Phys. B **29**, 57 (1996)], but disagree with the measured values [V. S. Kushawaha, Z. Phys. A **313**, 155 (1983)]. Comparison is also made for electron-capture cross sections into various nl levels of the target with the experimental and other theoretical results, whenever possible. The low-energy behavior of the excitation cross sections for both of the targets is also discussed.

DOI: 10.1103/PhysRevA.64.012721 PACS number(s): 34.70.+e, 34.50.−s

I. INTRODUCTION

A systematic study of collisions involving excited atoms finds wide applications in the field of plasma physics, lasers development, reaction kinetics, as well as in the atmospheric physics [1]. These investigations are of fundamental interest in understanding the elementary steps in photophysics and photochemistry [2]. The development of tunable dye lasers has also stimulated such investigations, because atomic species can now be prepared in well-specified quantum states. Also, by using polarized lasers it is now experimentally [3,4] possible to obtain with great accuracy the desired orientation and alignment of the electronic charge cloud of the initially excited target atom. These developments pose stringent tests on theoretical studies as their suitability and reliability can be critically examined at the fundamental levels.

In this context, the charge-transfer from excited alkali-metal atoms appears to be a tempting domain for theoretical study. A large number of experimental data on various aspects of such reactions, such as total and partial capture cross sections, alignment and anisotropy parameters, etc., on a number of excited alkali-metal targets provides an impetus to undertake a detailed systematic study on single charge-transfer processes. Saha and Weatherford [5] earlier initiated such an investigation for H^+-Li$(2p)$, employing a semiclassical impact-parameter method. In the present investigation, the next two members of the alkali-metal family are considered:

$$H^+ + Na(3p) \rightarrow H(nl) + Na^+, \tag{1a}$$

$$H^+ + K(4p) \rightarrow H(nl) + K^+. \tag{1b}$$

These reactions present the intriguing possibility of developing ultraviolet lasers since the $2p$ state decays radiatively, emitting Ly-α photons. The proton-sodium system, especially from the Na ground state, has drawn considerable attention over the past decade. At higher energies, Jain and Winter [6] have calculated total cross sections for electron transfer, target excitation, and ionization processes using a two-center coupled Sturmian pseudoapproach. At low energies, there are not many calculations [7–10] from the excited atomic Na target. Although these colliding pairs, along with Li-H^+, present an identical pseudo-one-electron picture, the details of the collision dynamics are expected to be different. As we move up in the alkali-metal series, we encounter a systematic change in the potential-energy surfaces, which can affect the final outcome of the charge-transfer reactions in Eqs. (1). Not only are the partial and total capture cross sections expected to exhibit a different energy dependence, but other collisional parameters involving alignment and orientation are also likely to exhibit substantial changes. These changes will appear in a systematic way, and should reflect the effect of having cores with various structures inside the pseudo-one-electron alkali-metal targets. To the best of our knowledge, such a systematic study is being proposed for the first time; an extension of our methodology to other higher members of the alkali-metal family is in order.

The present paper has been systematized as follows. A very brief description of the theoretical method is shown in the next section, in which we provide a detailed discussion regarding the alignment and orientation in this section. Various calculated parameters are presented in Sec. III, and a comparison with the experimental findings, whenever possible, is also made. Also in Sec. III, we present a comparative study among Li, Na, and K targets. The conclusions are

summarized in Sec. IV. Atomic units ($e=a_0=\hbar=m_e=1$) are used throughout, unless stated otherwise.

II. THEORETICAL METHOD

We have employed the impact-parameter, coupled-states method in the semiclassical formalism. In this scheme, which is well suited to the low-energy domain [11], the colliding pair is treated as a transient *diatomic molecule*, which in the asymptotic region dissociates to provide the entrance and various final channels of interest of the reaction. This molecular orbital (MO) prescription has been successfully used in the past to investigate charge-transfer reactions involving ion atoms and ion molecules as well [12–18]. Since the detailed theoretical method has been provided in a number of publications, we refer to one of our recent articles [5]. In the following, the basic ideas behind the approach are given.

A. Impact-parameter method

In this method, the internuclear movement of the two cores of the quasimolecule ($[(A^+ + H^+) - e^-]$; $A \equiv$ Na/K) is represented classically, whereas the electron's movement in the combined nuclear field is treated quantum mechanically. The effective binding of the electron in this system is simulated in the usual way; the pseudopotential method [19,20] is used to account for the short-range part of the effective interaction. To solve the time-dependent Schrödinger equation for the system, the total wave function is expanded in terms of the product of electronic wave functions and the electron translation factors (ETF); the latter is essential in order to satisfy Galilean invariance of the derived coupled equations [11,21]. At the same time, it also accounts for the physical transfer of the electron during the course of the collision from one core to the other. The derivations of the *optimized* form of the ETF used in this calculation were given by Kimura and Thorson [22] earlier; in their review article, Kimura and Lane [11] discussed the role of various terms with respect to **v** and demonstrated that at low energies the momentum term ($\approx$**v**) is significant. The electronic wave functions are obtained by the usual linear combination of atomic orbitals (LCAO) method, which along with the electronic energies $\varepsilon(R)$ have a parametric dependence on the internuclear separation, R, only (an adiabatic approximation).

The time-dependent Schrödinger equation leads to a set of coupled equations (for details, see Ref. [11]):

$$i\dot{a}_n = \sum_{k \neq n} \vec{V} \cdot (\vec{P} + \vec{A})_{kn} a_k + \varepsilon_n a_n , \tag{2}$$

where **P** and **A** represent the nonadiabatic couplings matrices and the EFT correction (to the first order in **V**), respectively; $\boldsymbol{\mathcal{E}}_n$ is the adiabatic electronic energy of the nth state. **V** represents the relative velocity and **a** denotes the required scattering amplitudes. These coupled equations, when solved numerically for each contributing impact parameter (b), yield the probability of transition from the initial state to a particular (kth) final state:

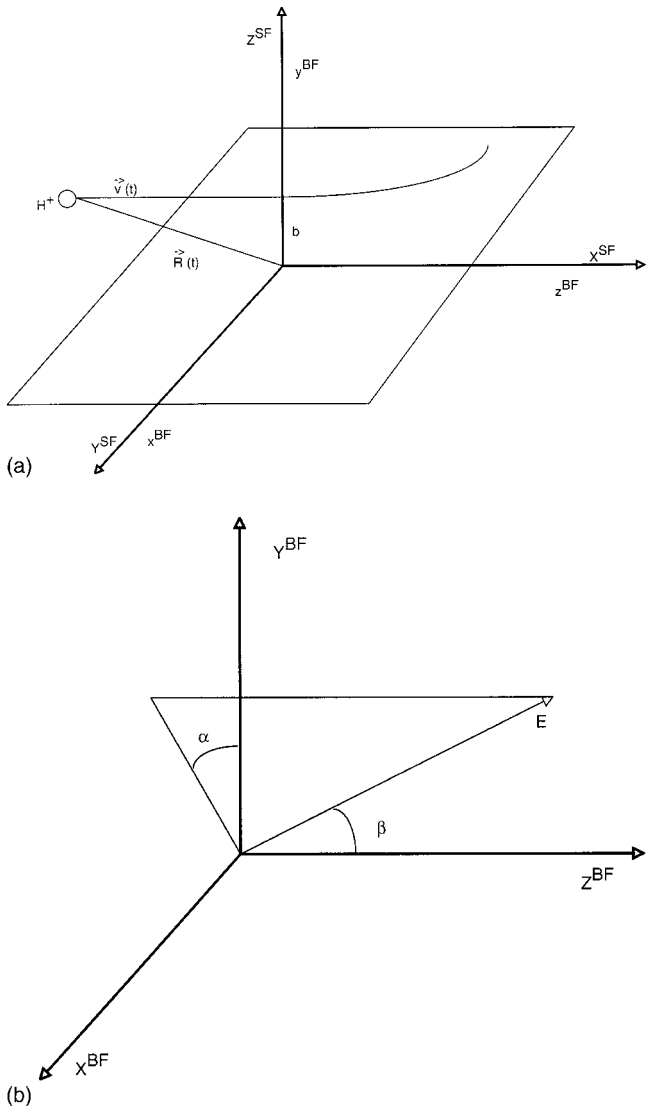

FIG. 1. (a) Collision geometry and reference frames for the scattering: the molecular body-fixed (BF) and the space-fixed (SF) coordinates are shown. The X^{SF} and z^{BF} axes are parallel to the velocity vector **v** of the incoming projectile; y^{BF} and Z^{SF} are perpendicular to the collision plane $[(X^{SF}-Y^{SF})$ or $(x^{BF}-z^{BF})]$. A projectile trajectory passing from the left side of the target is shown. (b) The polar coordinates of the electric vector $\mathbf{E}(\beta,\alpha)$.

$$P_k(E,b) = |a_k(+\infty,b)|^2 . \tag{3}$$

Integrating them over b, we obtain the relevant partial cross section at an impact energy E:

$$Q_k(E) = 2\pi \int db\, b P_k(E,b) . \tag{4}$$

B. Initial alignment and charge-transfer cross section

As the experimental observations are made in the space-fixed (SF) frame of reference, the transformation of coordinates is essential for comparison with the theoretically derived parameters that are evaluated generally in the body-fixed (BF) reference frame [see Fig. 1(a)]. Following Ref.

[5], the asymptotic form ($t\to\infty$) of the total wave function of the colliding system in the BF molecular frame can be written as

$$\Psi(t\to\infty)=\sum_n a_n^{\mathrm{BF}}\phi_n(r_A)\phi_n(r_H), \tag{5}$$

where a_n^{BF} is the scattering amplitude for the nth channel and ϕ_n are the wave functions of the target alkali-metal atoms and the incoming ions centered at the respective nuclei. In the BF frame, the molecular orbitals are transformed into the atomic orbitals (AO) by using the following relation:

$$\begin{bmatrix} |np_\Sigma\rangle \\ |np_{\Pi^+}\rangle \\ |np_{\Pi^-}\rangle \end{bmatrix}^{\mathrm{BF}} = \frac{1}{\sqrt{2}}\begin{bmatrix} \sqrt{2} & 0 & 0 \\ 0 & -1 & 1 \\ 0 & i & i \end{bmatrix}\begin{bmatrix} |np_0\rangle \\ |np_1\rangle \\ |np_{-1}\rangle \end{bmatrix}^{\mathrm{BF}}. \tag{6}$$

The corresponding scattering amplitudes from the BF-MO basis set to the SF-AO basis set are transformed via

$$\begin{bmatrix} a_0 \\ a_1 \\ a_{-1} \end{bmatrix}^{\mathrm{SF}} = \frac{1}{\sqrt{2}}\begin{bmatrix} 0 & 0 & \sqrt{2} \\ -1 & i & 0 \\ 1 & i & 0 \end{bmatrix}\begin{bmatrix} a_\Sigma \\ a_{\Pi^+} \\ a_{\Pi^-} \end{bmatrix}^{\mathrm{BF}}. \tag{7}$$

The reflection symmetry with respect to the collision plane leads to the simplification $a_{\Pi^-}^{\mathrm{BF}}=0$. In the SF-AO basis set, the wave function for $H(np)$ reduces to

$$\phi_{H(np)}^{\mathrm{SF}}=[a_{np_{+1}}^{\mathrm{SF}}|np_{+1}\rangle^{\mathrm{SF}}+a_{np_{-1}}^{\mathrm{SF}}|np_{-1}\rangle^{\mathrm{SF}}]/N, \tag{8}$$

where the normalization constant N is given by

$$N=\sqrt{[|a_{np_{+1}}^{\mathrm{SF}}|^2+|a_{np_{-1}}^{\mathrm{SF}}|^2]}. \tag{9}$$

To consider the dependence of the cross sections on the initial alignment angle β, let us assume that a linearly polarized laser beam has been used to prepare the $A(np)$ so that its charge cloud is aligned in a particular direction [Fig. 1(b)]. This alignment can be represented [5] by a pair of angles α and β, representing the direction of the electric vector $\vec{E}$ of the applied field. Therefore, the wave function of the initially excited target, $A(np)$, in the BF frame of reference becomes

$$|np\rangle_A=[\cos\beta+\sin\beta\cos\alpha+\sin\beta\sin\alpha]|nlm\rangle_A. \tag{10}$$

The probability of transition from the initial state $|nlm\rangle$ to any final state $|f\rangle$ at a particular impact parameter b and energy (E) will thus also be a function of α and β, and can be expressed as

$$P(b,E)=|\langle f|nlm\rangle|^2. \tag{11}$$

The experimental cross sections, corresponding to the conditions $\vec{E}\|Z^{\mathrm{SF}}$ and $\vec{E}\perp Z^{\mathrm{SF}}$, are expressed as $\sigma_\|$ and $\sigma_\perp$, respectively. They are given [5] by

$$\sigma_\|=\int_0^{2\pi}d\alpha\int_0^\infty db\,b[P(E,b;\beta=0,\alpha)] \tag{12a}$$

and

$$\sigma_\perp=\int_0^\infty db\,b\left[\int_0^\pi d\phi\,P(E,b,\beta=\pi/2,\alpha=0)+\int_0^\pi d\phi\,P(E,b,\beta=\pi/2,\alpha=\pi/2)\right], \tag{12b}$$

which, upon being integrated over the variable ϕ, yield

$$\sigma_\|=2\pi\int_0^\infty db\,b[P(E,b;\beta=0,\alpha)] \tag{13a}$$

and

$$\sigma_\perp=\pi\int_0^\infty db\,b[P(E,b;\beta=\pi/2,\alpha=0)+P(E,b,\beta=\pi/2,\alpha=\pi/2)]. \tag{13b}$$

Integrating over the azimuthal angle, the total cross section, for a given value of β can be expressed as

$$\sigma(E,\beta)=\sigma_\|\cos^2\beta+\sigma_\perp\sin^2\beta, \tag{14}$$

where both cross sections appearing on the right-hand side of Eq. (14) are evaluated using the MO basis in the expansion of the scattering wave function. Note that the $\sigma_\|$ is evaluated by taking Σ symmetries of the initial channel, whereas for $\sigma_\perp$ the initial state was a Π symmetry.

To obtain the final shell-resolved anisotropy parameter of the present reactions, the following expression [5] is employed:

$$A(n)=\frac{[\sigma_\Sigma(E)-\sigma_\Pi(E)]}{[\sigma_\Sigma(E)+\sigma_\Pi(E)]}. \tag{15}$$

It should be pointed out here that due to the rotational symmetry, σ_Σ and $\sigma_\|$ defined in the above relations are exactly equal to each other, but the same is not true for σ_Π and $\sigma_\perp$; for details, see Appendix A.

III. RESULTS AND DISCUSSION

The adiabatic potentials for $[(Na^++H^+)-e^-]$ and $[(K^++H^+)-e^-]$ are presented, respectively, in Figs. 2 and 3. From Fig. 2, where the adiabatic potential energies for $(NaH)^+$ are shown, it is evident that the couplings of the incident channels Na $3p\Sigma/\Pi$ with the molecular states correlating to the capture into the $n=2$ manifold of H provide the most important mechanism of charge transfer, but there is also a finite possibility of exoergic transitions leading to charge transfer into higher excited states (e.g., $n=3$ level) of the H atom. It is important to note that Allan [9] and Kimura *et al.* [8] have calculated the adiabatic energies for the $(NaH)^+$ molecule using the pseudopotential technique. Our results are in complete agreement with those of Kimura *et al.*, who also employed an *l*-dependent Gaussian-type pseudopotential for the Na^+ core ion, like ours. In his MO calculation, using an analytical expression [23] for the

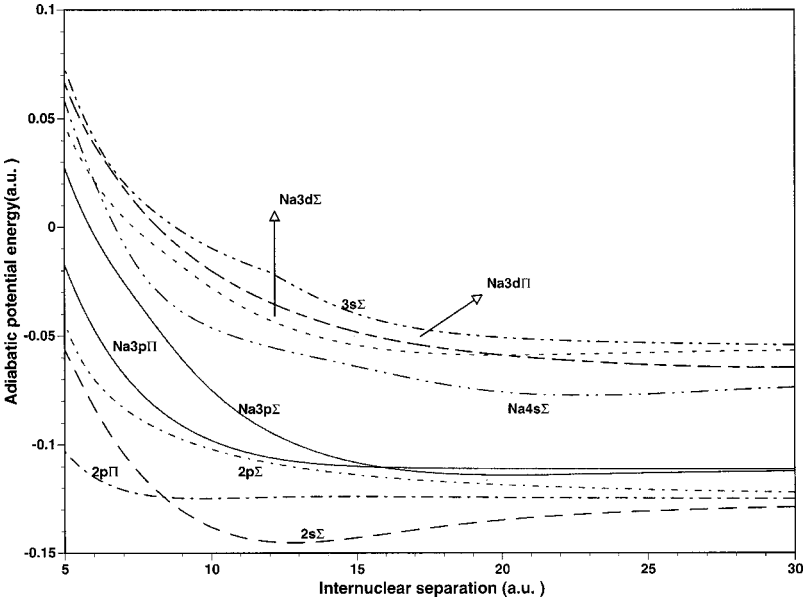

FIG. 2. Adiabatic potential-energy surfaces for the colliding system $H^+ + Na(3p)$. Various Σ and Π molecular states are shown explicitly.

e^--Na^+ interaction, Allan has obtained good agreement with the earlier results of Olson *et al.* [24].

The potential energies for $(NaH)^+$ differ in detail from that of $(LiH)^+$ in that the $Na(3p)$ level lies above the H $(n=2)$ channels whereas $Li(2p)$ lies below it. Thus the role of the radial couplings will be different in collision dynamics for both the targets. The region of strong avoided crossings, as compared to the $Li+H^+$ case [5], shifts to comparatively smaller internuclear separations, enhancing the possibility of electron transfer during the course of collision. Another important deviation from the Li target is the participation of the excited target states (namely, Na $4s\Sigma$ and Na $3d\Sigma/\Pi$) in the collision dynamics. As we will see later, this has a substantial influence on the electron-transfer processes for this pair.

For the other pair, $[(K^+ + H^+) - e^-]$, the adiabatic potential-energy surfaces move further up (see Fig. 3); thus the capture into the excited $n=3$ manifold of the H atom is expected to contribute more in the process of total electron transfer. Similar to the $Na+H^+$ collisions, the excited target states here also significantly influence the collision dynamics, and hence the n distribution of the charge-transfer cross sections.

From Fig. 2, it is evident that the initial channel Na $3p\Sigma$ shows an avoided crossing with the $2p\Sigma$ channel. The main gateway to the charge exchange at low energies is the radial coupling between these two channels. In Figs. 4 and 5, we have shown a few important radial couplings for both $Na+H^+$ and $K+H^+$ collisions, respectively. From Fig. 4, it is evident that in the lower R regions there are some sharply peaked coupling terms due to localized avoided crossing of the adiabatic potentials. However, at $R>20$ a.u., all couplings become very small. Courbin *et al.* [25], using a common translation factor (CTF), have studied the $Na+H^+$ system in the energy range $0.5 \leqslant E \leqslant 2$ keV. Using a different

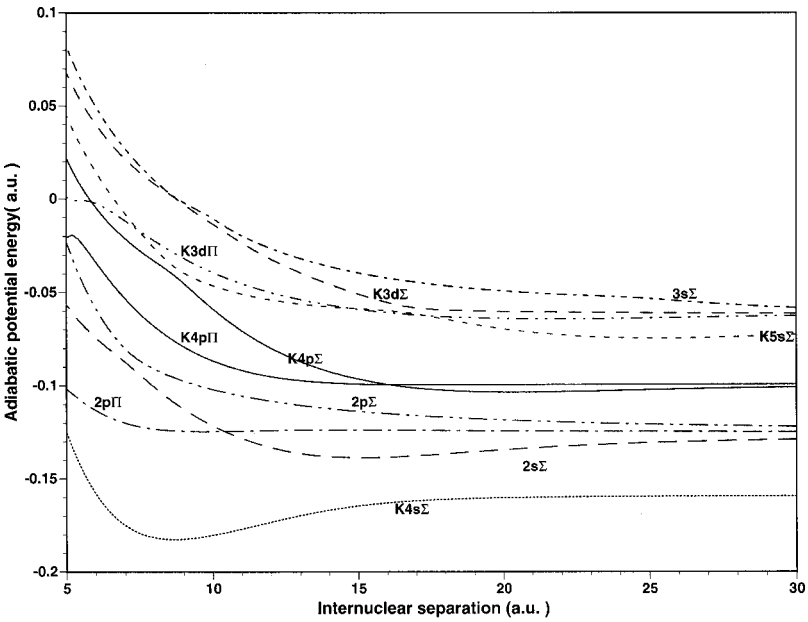

FIG. 3. Adiabatic potential-energy surfaces for the colliding system $H^+ + K(4p)$. Various Σ and Π molecular states are shown explicitly.

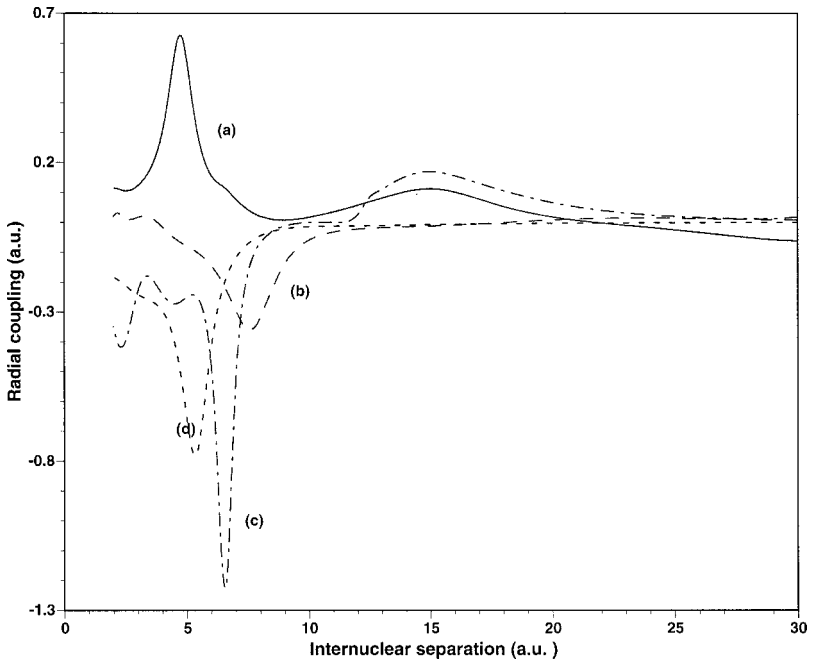

FIG. 4. Radial matrix elements (a.u.) for $H^+ + Na(3p)$ collisions. (a) $\langle Na\, 3d\Sigma | \partial/\partial R | Na\, 4s\Sigma \rangle$; (b) $\langle Na\, 4s\Sigma | \partial/\partial R | Na\, 3p\Sigma \rangle$; (c) $\langle H\, 3s\Sigma | \partial/\partial R | Na\, 3d\Sigma \rangle$; (d) $\langle H\, 2p\Sigma | \partial/\partial R | H\, 2s\Sigma \rangle$.

origin, the coupling matrix elements, especially in the important interaction region $5 < R < 18$ a.u., show different strength. A few important angular couplings for $Na + H^+$ and $K + H^+$ are plotted, respectively, in Figs. 6 and 7. In the lower R regions, there are a few strong couplings, which play important roles in the production of the H atom.

The convergence of our estimated cross sections with respect to the basis sets was also tested. The initial channel $Na\, 3p\Sigma/\Pi$ (see Fig. 2) exhibits no direct interaction with the molecular states correlating the capture into the $n=3$ manifold of the H atom. The population of H ($n=3$) is, therefore, expected to occur only through a number of multistep processes. However, to check the convergence of our calculations, we first carried out a few large calculations at some selected energy for reaction (1a). These studies involve a 13-state (eight Σ and five Π states) calculation, including the $n=3$ levels of H atom. Partial cross sections for the formation of the $n=3$ states of the H atom were found to be significantly smaller in magnitude, which enables us to reduce the number of states to be coupled together for evaluating various transitions relevant to the capture processes at such low energies. By carrying a nine-state (six Σ and three Π states) calculation, we have found that not only the total integrated cross sections but also the partial cross sections agree within 1% with the corresponding results obtained by the larger basis sets. At lower energies, the agreement was

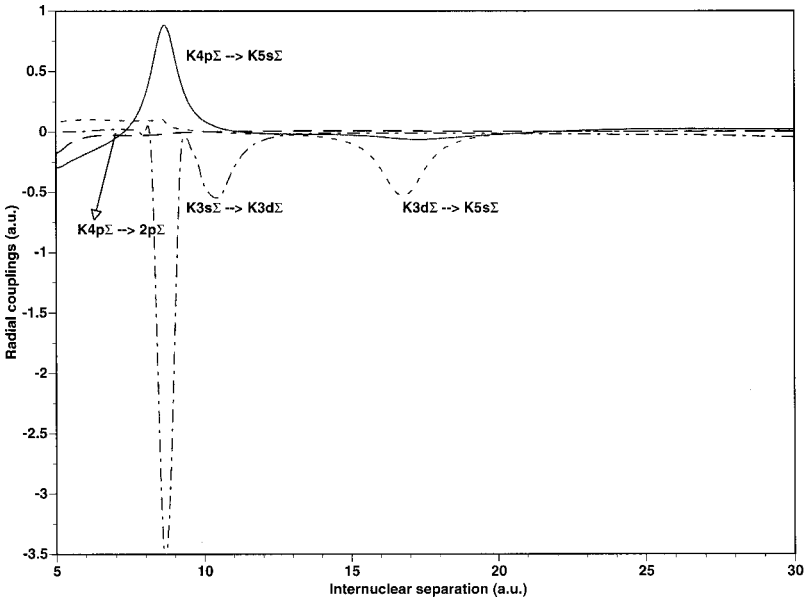

FIG. 5. Representative radial matrix elements (a.u.) for $H^+ + K(4p)$ collisions.

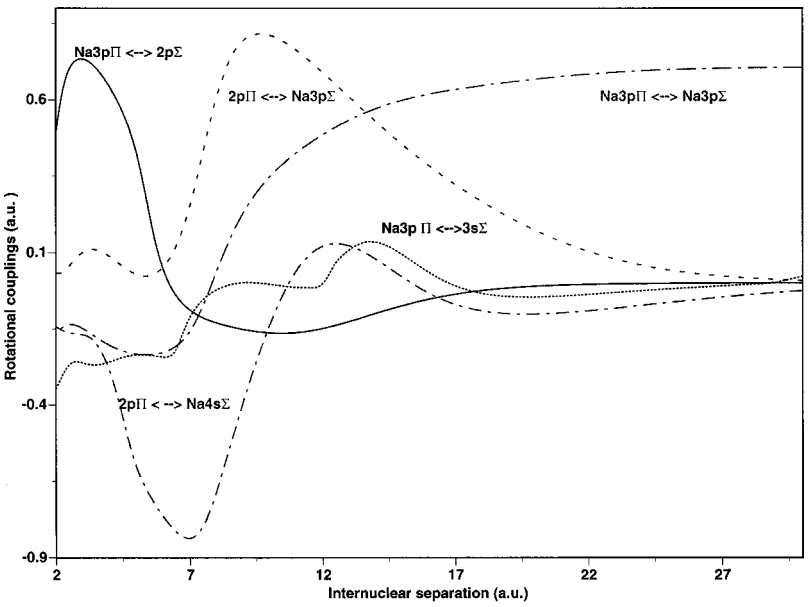

FIG. 6. Some important rotational matrix elements (a.u.) for $H^+ + Na(3p)$ collisions.

still better. We have done a similar convergence test for the other system ($K+H^+$); in order to retain the same 1% accuracy with respect to the larger basis set (fourteen states for the $K+H^+$ collision), we made a 10-channel calculation (see Fig. 3) comprising seven Σ and three Π states for the reaction (1b). It should be noted that the probabilities have been integrated employing Simpson's rule over the impact parameter b. We have also tested the b integration results using the trapezoidal rule. The agreement between the two findings was better than 5%. In order to obtain the 1% convergence of the integrated cross sections, we retain sufficient b points throughout our calculations.

A short comment on the use of the linear trajectory in this study seems imperative. In slow collisions, the active electron does not stay on a single Born-Oppenheimer energy surface, a representative of an eigenstate of the electronic Hamiltonian. The resulting near-adiabatic conditions, demonstrated through strong avoided crossings in the energy curves, induce electronic transitions. For the interacting pairs in which we are interested, a ''flurry of activity'' takes place around intermediate R values (see Figs. 2–5) where strong avoided crossings are observed. This region of interest is hardly expected to be influenced even if we consider a common potential curve trajectory for the approaching and the receding nuclei. We have made a few test calculations and found that the two results agree within 10% even at the lowest impact energy; the agreement improves at higher energies, as expected. It seems that below $E \leqslant 0.01$ keV amu^{-1}, a quantum-mechanical approach should be more appropriate.

The role of Σ and Π states as the incident channel for the charge-transfer reactions can be visualized through a study of the variation in the cross section for different alignment angles β [see Fig. 1(b)]. In order to look for systematic changes, if any, we show the β dependence of the dominant charge-transfer process, namely the population of H ($n=2$) in the $Na+H^+$ collision in Fig. 8. Here the rotational couplings attain greater significance in the dominant charge-transfer process; we find that except for a small energy re-

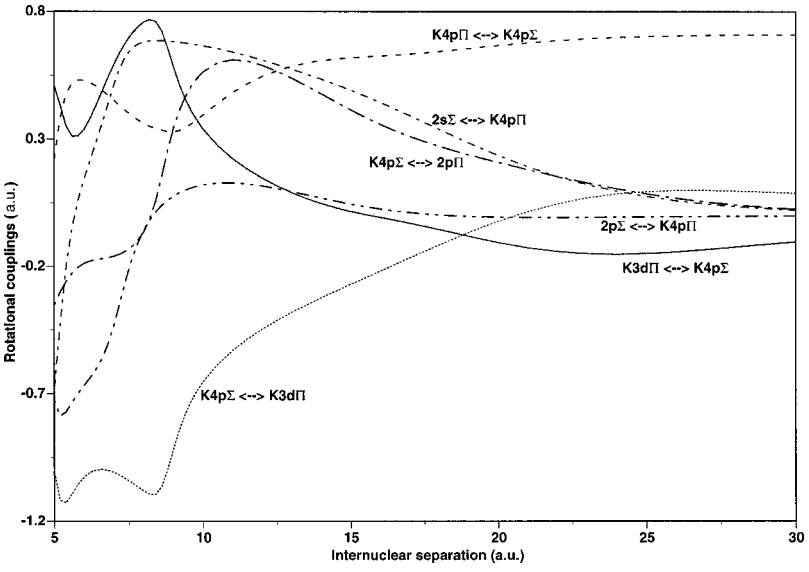

FIG. 7. Some important rotational matrix elements (a.u.) for $H^+ + K(4p)$ collisions.

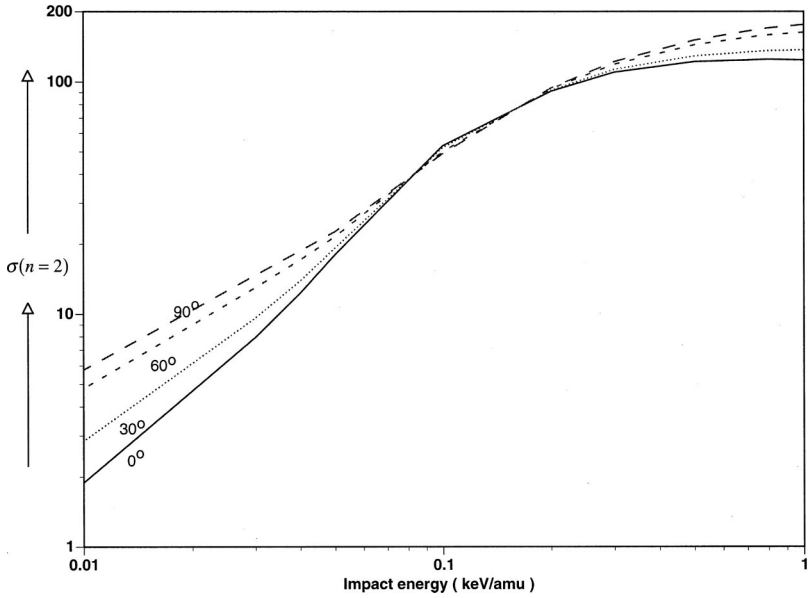

FIG. 8. β dependence of the cross section ($Å^2$) into $n=2$ manifold of H atom for the $Na+H^+$ pair.

gion around $E=0.1\,\mathrm{keV\,amu^{-1}}$, the charge cloud distribution normal to the internuclear axis provides a better option for electron transfer in this pair. But for the less important mode, which populates the $n=3$ manifold of the hydrogen atom, it is the initial Σ state that leads to larger capture cross sections. With increasing E, the cross sections corresponding to $\beta=0°$ and 90° tend to approach each other, suggesting that the relevant rotational couplings for this transition are also gaining strength (see Fig. 6). Since the capture into the $n=2$ manifold of the H atom far dominates the other transition mode, the total capture probability also follows the same trend as exhibited in Fig. 8.

The dominance of the rotational couplings (see Fig. 7) leading to the formation of H ($n=2$) throughout the region of our study is clearly demonstrated for the $K+H^+$ pair (Fig. 9). It is only at higher E that both types of charge distributions are found to provide nearly equal probability of electron transfer through this dominant mechanism. But the initial Σ state provides the preferential input for the population of H ($n=3$) in this reaction. Since this mode of charge transfer dominates over the formation of H ($n=2$) at lower energies, the total electron-transfer probability assumes an altogether different shape in terms of the alignment angle β. At $E\geqslant 0.5\,\mathrm{keV\,amu^{-1}}$, the contributions from both the initial Σ and Π states of the target are almost identical for the purpose of total electron capture.

For the $Li+H^+$ collision [5], the initial Σ state contributes more to the charge-transfer reaction at lower energies (E

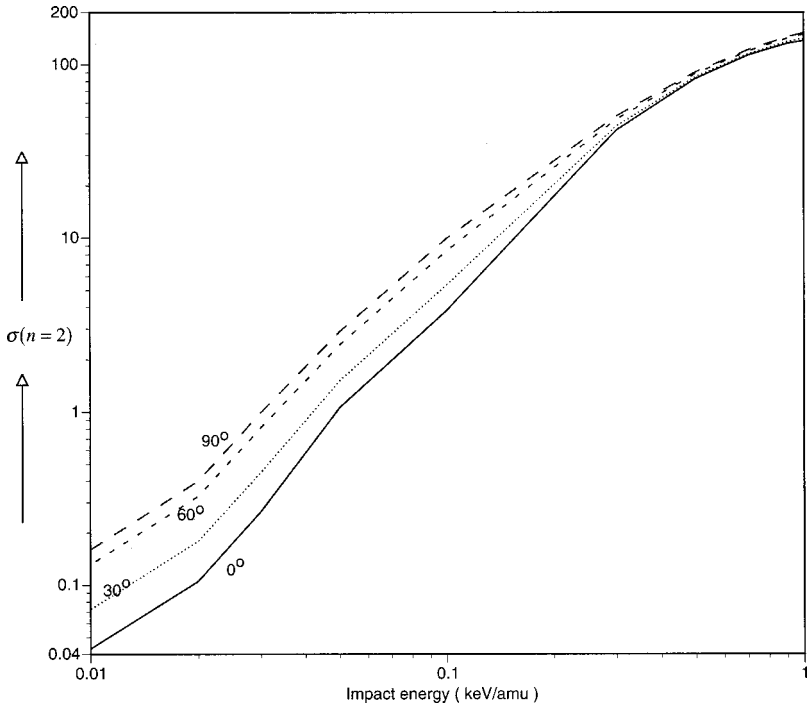

FIG. 9. β dependence of the cross section ($Å^2$) into $n=2$ manifold of H atom for the $K+H^+$ pair.

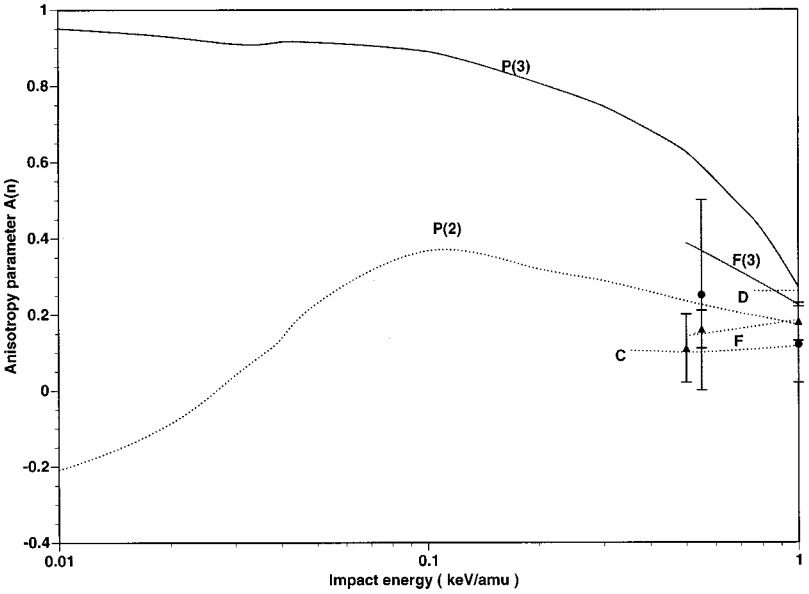

FIG. 10. Anisotropy parameters $A(n=2)$ and $A(n=3)$ for the $Na+H^+$ pair. $P(2)$ and $P(3)$ refer to present calculations for $n=2$ and 3 manifolds, respectively; experiments (triangle, $n=2$; circle, $n=3$) are from Ref. [26]; *C* [25], *F* [27], and *D* [28] curves are theoretical estimates of $A(n=2)$; $F(3)$ is the theoretical calculation for $A(n=3)$ [28].

$\leqslant 0.06\,\mathrm{keV\,amu^{-1}}$). At $0.05 \leqslant E \leqslant 0.06\,\mathrm{keV\,amu^{-1}}$, it was found that the contributions due to the initial Σ and Π states were nearly equal, producing *isotropic alignment*. However, for the next alkali-metal member (i.e., Na), we observe this isotropy in a very limited energy region between 0.08 and 0.2 $\mathrm{keV\,amu^{-1}}$. As we move up to the next target, the Π configuration remains always dominant, and a near-isotropy is obtained only at higher energies ($E > 0.3\,\mathrm{keV\,amu^{-1}}$).

Another way of looking into the collision dynamics of these charge-transfer processes is to evaluate the final-state principal shell-resolved anisotropy parameter [Eq. (15)]. Figure 10 depicts the anisotropy parameter for the $Na+H^+$ system, for which a couple of measurements [26–28] are available. But as can be seen from this figure, there are no other theoretical or experimental results at lower energies, especially at $E \leqslant 0.3\,\mathrm{keV\,amu^{-1}}$. Our results for capture into both the $n=2$ and $n=3$ manifolds of H atoms are found to agree with the experimental values [26,27] at higher energies. The anisotropy parameters for the formation of H ($n=2$) in this reaction are slightly larger than those of Courbin *et al.* [25] and Fritsch [29]. It should be mentioned here that Courbin *et al.* have employed a similar MO approach to evaluate these parameters. Our MO approach, however, differs in two ways from their calculations. Instead of using a common translation factor (CTF), we use an ETF that can simulate the molecular aspect of the translation of the electron between the two cores, and in contrast to their model potential, we have invoked the method of pseudopotential to account for the electron binding in the quasimolecule. Moreover, we have extended our calculations to much lower energies and have also explicitly obtained the contribution of the capture into the $n=3$ manifold of H. The present anisotropy parameters for the dominant charge-transfer mechanism (for $n=2$ level) are slightly smaller than those given in Ref. [30]. At higher energies, for the population of H ($n=3$) our results agree well with the findings of Fritsch [29], which is the only other available theoretical calculation for this system. Note also the limitation of the AO approach at lower energies.

For a comparative study, we present the anisotropy parameters for both Na and K atoms colliding with H^+ in Fig. 11. In this figure, we have also included these parameters for populating the excited states (denoted by ''ex'' in the corresponding curves) of these targets, for which, to the best of our knowledge, no other theoretical or experimental results are available in the literature. At low energies ($E \leqslant 0.03\,\mathrm{keV\,amu^{-1}}$), $A(2)$ for both Na and K starts with a negative value, while $A(3)$ remains positive throughout the studied energy regime. Only a qualitative agreement between the two targets for $A(2)$ is observed, except at higher energies, where the anisotropy parameters take comparable values. At low energies, the projectile can feel the details of ion-target interactions, and consequently a large difference in $A(2)$ is observed. It should be remembered here that both of these targets possess similar core structure; the excited electron is backed by a completely filled *p* shell. For electron capture into $n=3$, we noticed that at low energies ($E \leqslant 0.2\,\mathrm{keV\,amu^{-1}}$), $A(3)$ for both the Na and K target takes comparable values and shows a similar energy dependence. However, at higher energies there are differences observed in $A(3)$ for the electron capture from both the Na and K targets. It should be pointed out here that the $Li+H^+$ system exhibited a completely different behavior; the anisotropy parameter $A(2)$ for this system remained positive throughout the investigated low-energy region [5]. In terms of the studied anisotropy parameters $A(2)$ and $A(3)$, it seems that the role of the target core is quite different for both targets. A generalization is yet not possible until further studies involving the correlation effect due to the core size and structure are carried out in more detail on other alkali-metal targets (Rb, Cs, etc.), which we intend to do in the near future.

In order to test our calculations at low energies we have compared our results in Fig. 12 with the only available quantal calculations of Croft and Dickinson [31] for the Ly-α emission in the case of $Na+H^+$ collisions. The experimental results [32] are also depicted in the same figure. The earlier semiclassical MO results [10] are also shown in the same figure for comparison. Following Allan *et al.* [10], our

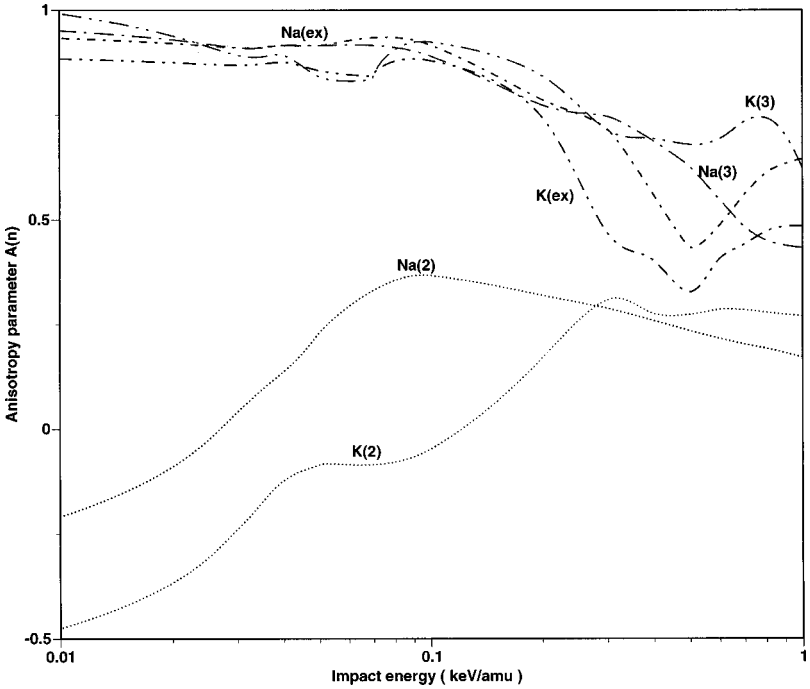

FIG. 11. Comparison of anisotropy parameters for the $Na+H^+$ and $K+H^+$ pairs. The present calculated parameters for the population of $n=2$ and 3 manifold of the H atom, as well as for the excitation of the target (ex) are shown clearly.

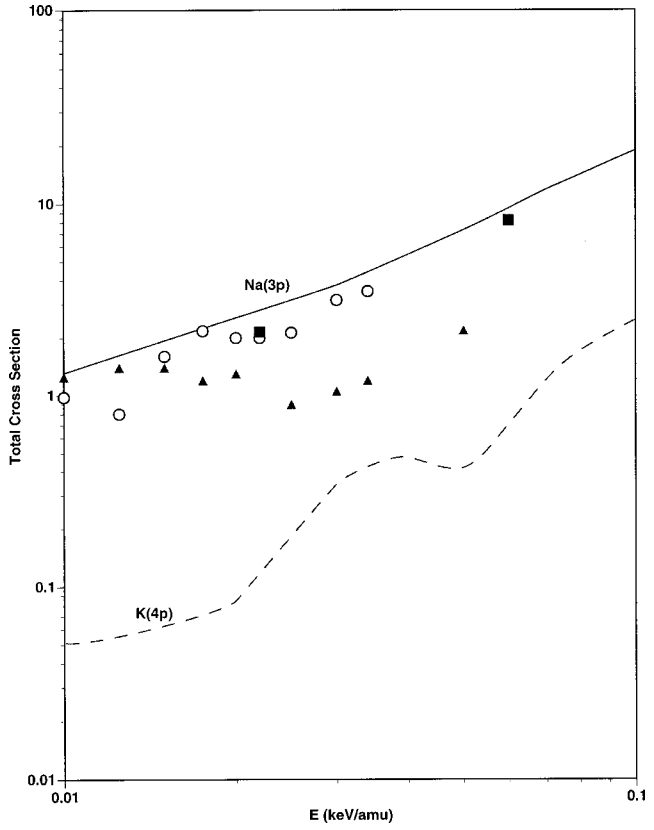

FIG. 12. Comparison of total charge-transfer cross section ($Å^2$) for Ly-α production (perpendicular to the incident beam). Solid line, present results for $H^+ + Na(3p)$ collisions; open circle, theoretical quantal results [31]; solid triangle, experimental results [32]; solid square, theoretical semiclassical results [10]; dashed curve, present results for $H^+ + K(4p)$ collisions.

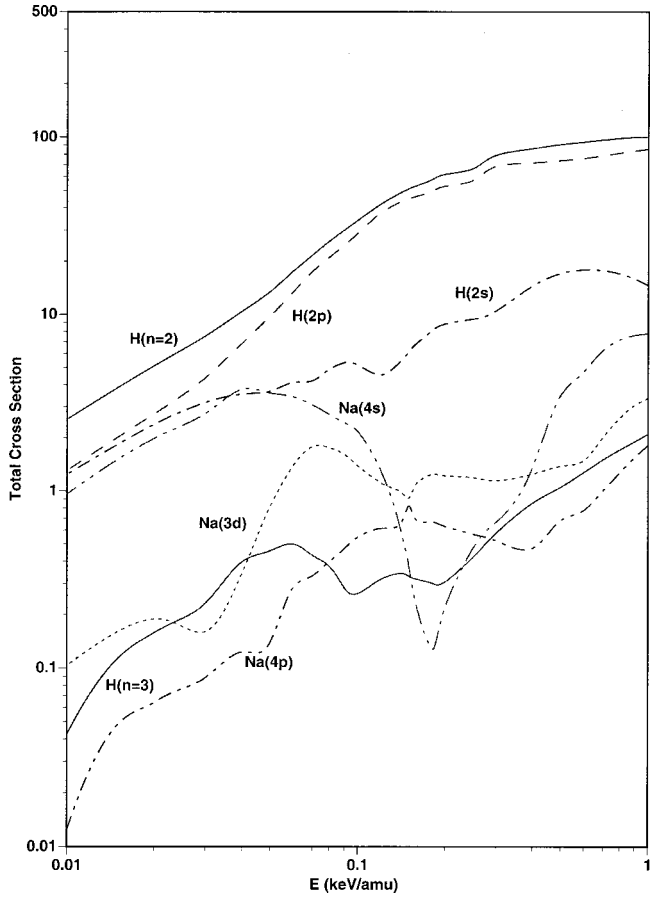

FIG. 13. The excitation and one-electron capture cross sections ($Å^2$) for H^+ in $Na(3p)$ collisions as a function of energy. The capture into various l states is shown separately. Proton impact excitation cross sections to $Na(4s)$, $Na(3d)$, and $Na(4p)$ states from the initial $Na(3p)$ state of the target are shown explicitly.

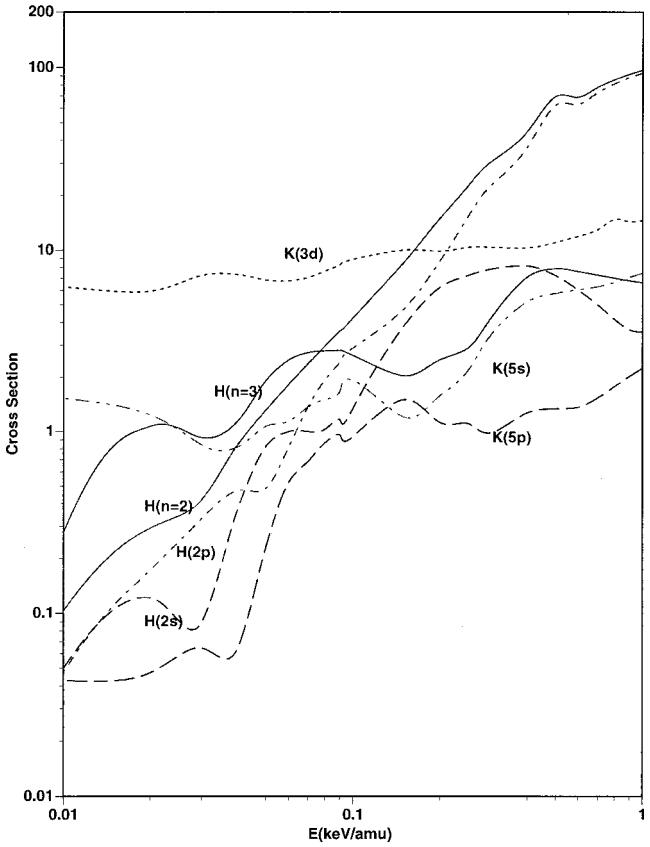

FIG. 14. The excitation and one-electron capture cross sections ($Å^2$) for H^+ in $K(4p)$ collisions as a function of energy. The capture into various l states is shown separately. Proton impact excitation cross sections to $K(5s)$, $K(3d)$, and $K(5p)$ states from the initial $K(4p)$ state of the target are shown separately.

present cross sections are weighted to account for the observation of Ly-α radiation perpendicular to the laser beam. The agreement with the quantal results is good. Our cross sections for charge transfer from the $Na(3p)$ lie above the experimental results and are supported by the results of Allan *et al.* and Croft and Dickinson in that they both disagree with the experimental findings [32]. At higher energies, our cross sections agree closely with the results of Allan *et al.* To the best of our knowledge, there are no theoretical and experimental results available for the $K+H^+$ collisions to compare with. In the case of $K+H^+$ collisions, the cross sections for Ly-α emission perpendicular to the incident beam are comparatively small (see Fig. 12).

In Figs. 13 and 14, we present our calculated cross sections for the electron capture into various *nl* levels and also for the excitation of Na and K atoms, respectively. From Fig. 13, it is evident that the capture into the $n=2$ manifold of H remains dominant throughout the studied energy region. The population of the $n=3$ levels of the H atom is almost an order of magnitude smaller than that of the $n=2$ manifold. The excitation cross sections to $Na(4s)$, $Na(3d)$, and $Na(4p)$ states from the initial $Na(3p)$ state are also very small. Except at $0.1 \leqslant E \leqslant 0.2$ keV amu^{-1}, the excitation to $Na(4s)$ remains larger as compared to both $Na(3d)$ and $Na(4p)$ excitations. In Fig. 14, we have noticed that the $n=3$ manifold of H remains preferentially populated in this reaction. At higher energies, the formation of the H ($n=2$) atom dominates. In the $H^+ + K(4p)$ collisions, the excitation of the target also plays an important role. Even at lower energies, the excitation to $K(3d)$ as well as $K(5s)$ becomes important. Throughout the energy range, the contribution to the excitation of the $K(3d)$ state is significant.

In Figs. 15 and 16, we present our results for the total capture cross sections for the reaction (1a), for which there are some recent measurements [3]. In agreement with the experiment and other theoretical studies [10,25], we find that the single electron capture is highly state-selective in the low-energy region. At $E=0.35$ keV amu^{-1}, the experimental findings overestimate all theoretical results. But at $E \geqslant 0.5$ keV amu^{-1}, our results are in very good agreement with the measurements. We also extend our calculations to lower energies, where, to the best of our knowledge, there are no other theoretical or experimental results available.

IV. CONCLUSION

We have investigated the process of single-electron transfer from the first excited p states of both Na and K atoms to

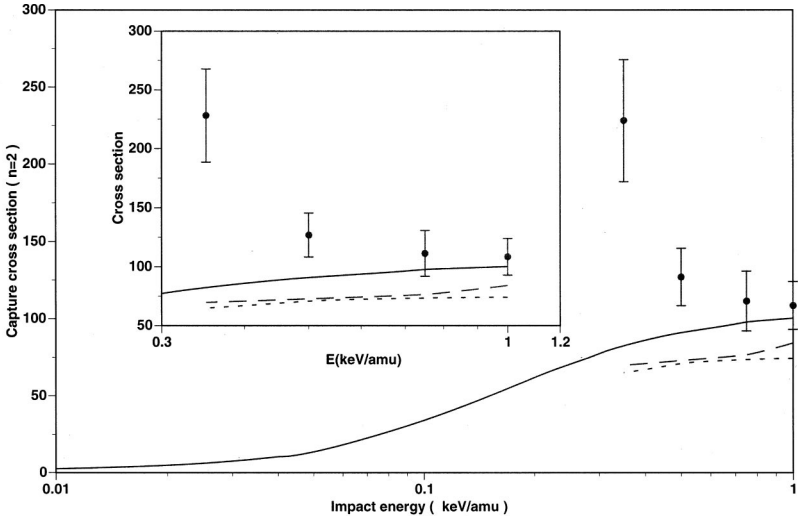

FIG. 15. Comparison of capture cross section ($Å^2$) into $n=2$ manifold of the H atom in the reaction (1a). Theoretical data: solid line, present; small dashed curve, Ref. [25]; long dashed curve, Ref. [10]. The experimental data (solid circles) are from Ref. [3].

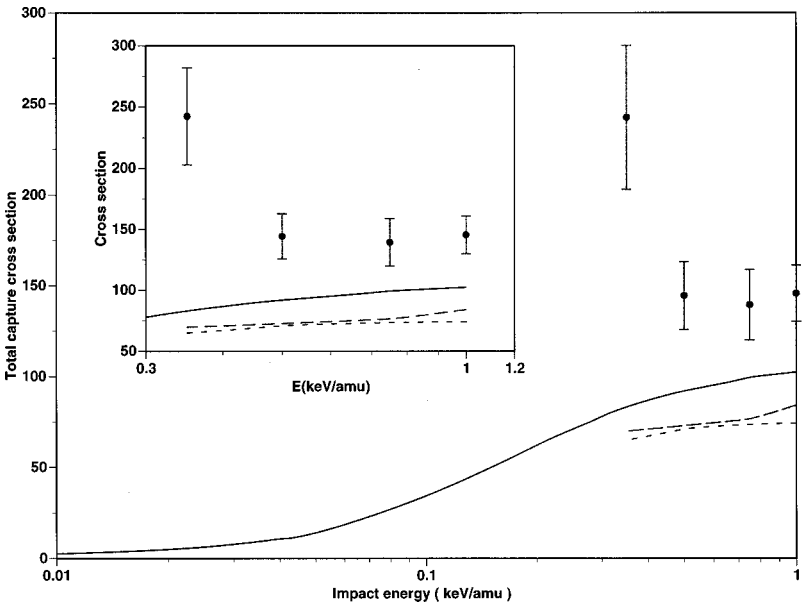

FIG. 16. Comparison of total capture cross section ($Å^2$) for $H^+ + Na(3p)$ collisions. Theoretical data: solid line, present; small dashed curve, Ref. [25]; long dashed curve, Ref. [10]. The experimental data (solid circles) are from Ref. [3].

the incident H^+ in the low-energy region by invoking a MO approach including the ETF in the framework of the impact-parameter formalism. The present calculation is able to account for the measured values of the partial and the total capture cross sections for the $Na+H^+$ collisions. The good agreement between our results with the only quantal calculations for the Ly-α emission in the case of $Na+H^+$ collisions supports the fact that our MO approach is appropriate to investigate the low-energy domain. We also successfully explore the role of orientation and alignment of these charge-changing reactions, especially in the low-energy region, where there are no other results available. Use of a fairly large basis set enables us to study the possible role of the excited states of the targets in such reactions. In addition to the anisotropy parameter $A(n)$, we also report the cross sections for electron capture into various *nl* levels and also for excitation of the target. The anisotropy parameters for the transitions leading to the excited target states of both the parent Na and K atoms have also been presented. A comparative study between these exhibits a systematic variation in those parameters, suggesting that the core structure of the target is playing some role in these collisions. Further study on other alkali-metal targets is, however, needed before a definite correlation, if any, can be revealed. At low energies, the single-electron capture is highly state-selective. The important couplings occur at intermediate values of *R*, where strong avoided crossings are observed in the potential-energy curves; in this region, the choice of common potential curve trajectory does not effect results more than 10% even at the lowest energies. We hope the present investigation will generate renewed interest in the experimental studies of the influence of the alignment of the excited target on charge exchange collisions.

ACKNOWLEDGMENTS

The authors would like to thank Professor Neal F. Lane for many helpful and constructive suggestions. B.C.S. wishes to acknowledge the financial support from the Research Corporation, NASA (Grant No. NAG5-10148), the NSF-CREST cooperative agreement HDR-9707076, and the Army High Performance Computing Research Center under the auspices of the Department of the Army, Army Research Laboratory cooperative agreement No. DAAH04-95-2-0003/Contract No. DAAH04-95-C-0008, the content of which does not necessarily reflect the position or the policy of the government, and no official endorsement should be inferred. A grant in supercomputer time from the Florida State University is also acknowledged.

APPENDIX

Let us consider an aligned *p* atomic orbital, with respect to which an incoming particle arrives at a point (b,ϕ) [see Fig. 1(a)]. The initial channel can, therefore, be decomposed according to

$$|\Pi\rangle = |\Pi^+\rangle \cos\phi + |\Pi^-\rangle \sin\phi. \tag{A1}$$

The scattering atomic amplitude a_Π and the total cross section σ_Π are then given by

$$a_\Pi(b,\phi) = a_{\Pi^+}(b)\cos\phi + a_{\Pi^-}(b)\sin\phi \tag{A2}$$

and

$$\sigma_\Pi = 2\pi \int_0^\infty |a_\Pi(b)|^2 b\, db, \tag{A3}$$

where the integration over the azimuthal angle has already been performed. Substituting Eq. (A2) into Eq. (A3) leads to a simplified expression,

$$\sigma_\Pi = \frac{1}{2}\left(2\pi \int_0^\infty |a_{\Pi^+}(b)|^2 b\, db + 2\pi \int_0^\infty |a_{\Pi^-}(b)|^2 b\, db \right) \tag{A4}$$

because the interference term cancels out. As noted earlier, the reflection symmetry with respect to the collision plane introduces a simplification in our formulation, reducing the second term to zero. Consequently, the atomic cross section finally turns out to be

$$\sigma_{\Pi} = \tfrac{1}{2}\sigma_{\Pi^+}, \tag{A5}$$

which, in the present study, amounts to

$$\sigma_{\Pi} = \tfrac{1}{2}\sigma_{\perp}. \tag{A6}$$

[1] J. Schweinzer, D. Wutte, and H. P. Winter, J. Phys. B **27**, 137 (1994).
[2] R. K. Janev and H. Winter, Phys. Rep. **117**, 265 (1985).
[3] T. Royer, D. Dowek, J. C. Houver, J. Pommier, and N. Andersen, Z. Phys. D: At., Mol. Clusters **10**, 45 (1988); U. Müller, H. A. J. Meijer, N. C. R. Holme, M. Kmit, J. H. V. Lauritsen, J. O. P. Pedersen, C. Rihter, J. W. Thomsen, N. Andersen, and S. E. Neilsen, *ibid.* **33**, 187 (1995).
[4] R. Hippler, J. Phys. B **26**, 1 (1993).
[5] B. C. Saha and C. A. Weatherford, J. Mol. Struct.: THEOCHEM **388**, 97 (1996).
[6] A. Jain and T. G. Winter, Phys. Rev. A **51**, 2963 (1995).
[7] C. Kubach and V. Sidis, Phys. Rev. A **23**, 110 (1981).
[8] M. Kimura, R. E. Olson, and J. Pascale, Phys. Rev. A **26**, 1138 (1982).
[9] R. J. Allan, J. Phys. B **19**, 321 (1986).
[10] R. J. Allan, R. Singhal, and D. R. Flower, J. Phys. B **19**, L251 (1986).
[11] M. Kimura and N. F. Lane, Adv. At., Mol., Opt. Phys. **26**, 79 (1989).
[12] B. C. Saha and A. Kumar, J. Phys. B **31**, L613 (1998).
[13] A. Kumar, B. C. Saha, and C. A. Weatherford, Int. J. Quantum Chem. **70**, 909 (1998).
[14] B. C. Saha, N. F. Lane, and M. Kimura, Phys. Rev. A **44**, R1 (1991).
[15] A. Kumar and B. C. Saha, J. Phys. B **31**, L937 (1998).
[16] A. Kumar and B. C. Saha, Phys. Rev. A **59**, 1273 (1999).
[17] B. C. Saha and A. Kumar, J. Mol. Struct.: THEOCHEM **487**, 11 (1999).
[18] B. C. Saha and A. Kumar, Int. J. Quantum Chem. **75**, 385 (1999).
[19] J. N. Bardsely, Case Stud. At. Phys. **4**, 299 (1974).
[20] J. Pascale, Phys. Rev. A **28**, 632 (1983).
[21] J. B. Delos, Rev. Mod. Phys. **53**, 287 (1981).
[22] M. Kimura and W. R. Thorson, Phys. Rev. A **24**, 1780 (1981); **24**, 3019 (1981).
[23] M. Klapisch, thesis, Université de Paris–Sud, Orsay (1969).
[24] R. E. Olson, R. P. Saxon, and B. Liu, J. Phys. B **13**, 297 (1980).
[25] C. Courbin, R. J. Allan, P. Salas, and P. Wahnon, J. Phys. B **23**, 3909 (1990).
[26] C. Richter, D. Dowek, J. C. Houver, and N. Andersen, J. Phys. B **23**, 3925 (1990).
[27] J. W. Thomsen, Can. J. Phys. **74**, 950 (1996).
[28] M. Gieler, F. Aumayr, M. Hutteneder, and H. Winter, J. Phys. B **24**, 4419 (1991).
[29] W. Fritsch, Phys. Rev. A **30**, 1135 (1984).
[30] A. Dubois, S. E. Nielsen, and J. P. Hansen, J. Phys. B **26**, 705 (1993).
[31] H. Croft and A. S. Dickinson, J. Phys. B **29**, 57 (1996).
[32] V. S. Kushawaha, Z. Phys. A **313**, 155 (1983).